catalysts

MDPI

Article

The Use of Tunable Optical Absorption Plasmonic Au and Ag Decorated TiO_2 Structures as Efficient Visible Light Photocatalysts

Xiaohong Yang [1,2,3], Yan Wang [2], Lingtong Zhang [2], Haitao Fu [1,2,*], Peng He [2], Dezhi Han [4], Tom Lawson [5] and Xizhong An [2,*]

1 Key Laboratory for Ecological Metallurgy of Multimetallic Mineral, Ministry of Education, Northeastern University, Shenyang 110819, China; yangxh@smm.neu.edu.cn
2 School of Metallurgy, Northeastern University, Shenyang 110819, China; wangyan18996@gmail.com (Y.W.); zlingtong007@gmail.com (L.Z.); LNAShepeng@outlook.com (P.H.)
3 Institute of Molecular Medicine, Sechenov First Moscow State Medical University, Moscow 119991, Russia
4 College of Chemical Engineering, Qingdao University of Science and Technology, Qingdao 266042, China; handzh@qust.edu.cn
5 ARC Centre of Excellence for Nanoscale BioPhotonics (CNBP), Department of Physics and Astronomy, Macquarie University, Sydney, New South Wales 2113, Australia; thomas.lawson@mq.edu.au
* Correspondence: fuht@smm.neu.edu.cn (H.F.); anxz@smm.neu.edu.cn (X.A.)

Received: 16 December 2019; Accepted: 15 January 2020; Published: 20 January 2020

Abstract: Exploring solar-excited heterogeneous photocatalysts by taking advantage of surface plasmon resonance (SPR) has drawn growing research attention. As it could help to pave the way for global sustainable development. The decoration of TiO_2 particles with noble metals possessing SPR effects is regarded as one of the most effective solutions. The perfect match of the SPR absorption band with the spectrum of incident light is an essential factor for plasmonic enhancement. However, modifying with sole noble metal is often limited as it tunes wavelength of only several nanometers. To overcome this drawback, an alternative approach can be offered by decoration with more than one noble metal. For instance, Au-Ag co-decoration displays greatly adjustable, composition-dependent SPR agent over a broad range of the visible light spectrum (ca. from 415 to 525 nm). Hence Au-Ag complex is a remarkable candidate for tuning the photo adsorption of TiO_2 from UV to visible light. This study presents a novel and tailored method for the fabrication of Au-Ag co-modified TiO_2 particles, and how Au-Ag dependent SPR was applied as the visible light-responsive TiO_2 based photocatalysts in a simple but reliable way. The fabricated Au-Ag co-decorated TiO_2 ($Au_xAg_{(1-x)}/TiO_2$) was characterized and proved to own excellent stability and large specific surface area. The optimization of these particles against the wavelength of maximal solar light intensity was confirmed by photo degradation of methylene blue under visible light radiation. This work may provide further insight into the design of TiO_2-based composites with improved photocatalytic properties for environmental remediation and renewable energy utilization.

Keywords: sol-gel process; Au-Ag co-modified TiO_2 composites; surface plasma resonance; visible light photocatalyst

1. Introduction

As the first reported photocatalyst, TiO_2 has received extensive attention owing to its strong photo oxidization capacity and excellent long-term stability [1]. However, because of its large bandgap, (ca. 3.2 eV), TiO_2-involved photocatalysis has been widely regarded as a UV-light-triggered oxidation-reduction processes. Yet, it is well-known that the UV wavelength only accounts for

less than 5% of the entire solar spectrum energy [2], and this highly restricts the usefulness of TiO_2-based photocatalysts as a renewable energy technology in such areas as environmental remediation, self-cleaning surface, CO oxidation and H_2 production [3–6]. Thus, the development of a visible light-responsive TiO_2-based photocatalyst would be highly desirable. A number of strategies have been reported to extend its adsorption range into the visible light spectrum by changing the bandgap of semiconductors, including replacing O atom in TiO_2 with C or N [7,8], doping with metal element, such as Sb and V [9,10], decorating with other metal oxides [11,12], or preparing hydrogenated black-TiOx structures [13]. Among these, engineering of TiO_2 by decorating plasmonic metallic nanoparticles with Ag or Au is a particularly promising approach [14].

Surface plasmon resonance (SPR) is defined as the collective oscillation of valence electrons induced by a resonant photon. The resonant photon wavelength varies with the metal tested [15]. The resonant wavelength and the resulting SPR intensity are dependent on the structure, as well as the size and shape of the metallic nanoparticles [16,17]. By manipulating the above factors of plasmonic nanoparticles, it is possible to prepare nanostructures that interact across the whole solar spectrum [18,19]. However, the decoration of TiO_2 with the single noble metal is limited to several nanometers of wavelength tuning [20–22]. To overcome this, two noble metals can be added to the composite. For example, Au-Ag binary nanoparticles are able to exhibit composition-dependent SPR maxima over a wide range of the visible light spectrum (Ca. from 415 to 525 nm) [23,24]. Hence, Au-Ag nanoparticles make a competent candidate for harvesting the photoabsorption of TiO_2 in the spectrum of solar light via their plasmonic enhancement properties [25].

Metallic Au and Ag nanoparticles were synthesized by many groups [26–29]. Most of these describe Au-Ag particle fabrication in aqueous solutions [30,31]. Sun's group however, described the fabrication of monodisperse Au-Ag nanoparticles in an organic solvent [32]. They tuned the Au-Ag nanoparticles by changing the ratio of the precursors in the reaction. This resulted in a synchronous change in the size of Au-Ag particles, and consequently a change in the variation of their SPR frequency. Liu et al. reported a milder method for synthesizing Au-Ag particles that used an organic agent. The resulting particles were highly monodispersed and had a particle size from 6 to 13 nm [33]. They adjusted the size as well as the SPR frequency by changing the ratios of the metals added and by changing the surfactants used. Despite these reported successes, the efficient simple manufacture of Au-Ag binary nanoparticles for the purpose of tuning of SPR through Au-Ag composition remains a research goal.

This study reports a tailored synthetic method to prepare Au-Ag binary nanoparticles and their resulting SPR properties can be applied to produceTiO_2-based photocatalysts with SPR at specific, desired visible light wavelengths in a straightforward way. The morphology and composition of the Au-Ag co-decorated TiO_2 ($Au_xAg_{(1-x)}/TiO_2$) were characterized by TEM, HRTEM, SEM, and XRD. The optical properties were investigated by UV-vis spectroscopy. Furthermore, the as-prepared Au-Ag co-decorated TiO_2 ($Au_xAg_{(1-x)}/TiO_2$) composites with their adsorption band overlap with the wavelength of the strongest solar light intensity were demonstrated via the photodegradation of methylene blue under visible light illumination. The mechanism of enhanced photocatalytic performance is eventually discussed.

2. Results and Discussion

2.1. Composition Analysis

The XRD technique confirmed the composite of the as-prepared particles. In order to tune the molar ratio between Au and Ag in the composites of Au-Ag/TiO_2, the total amount of Au-Ag to TiO_2 was fixed to an optimized value (2.25 wt%), which was determined in our preliminary study. $Au_xAg_{(1-x)}/TiO_2$, (x = 0, 0.2, 0.4, 0.6, 0.8 and 1) was used to calculate the different molar ratio between Au and Ag. $Au_xAg_{(1-x)}/TiO_2$, (x = 0, 0.2, 0.4, 0.6, 0.8 and 1) can separately represent the composites of TiO_2 only doped with 2.25 wt% Ag (x = 0), TiO_2 doped with 0.35 wt% Au and 1.9 wt% Ag (x = 0.2),

TiO_2 doped with 0.74 wt% Au and 1.51 wt% Ag (x = 0.4), TiO_2 doped with 1.18 wt% Au and 1.07 wt% Ag (x = 0.6), TiO_2 doped with 1.67 wt% Au and 0.61 wt% Ag (x = 0.8), and TiO_2 only doped with 2.25 wt% Au (x = 1). Figure 1 shows the XRD patterns of pure TiO_2 (black line) and 1.18 wt% Au-1.07 wt% Ag co-decorated TiO_2 particles ($Au_xAg_{(1-x)}/TiO_2$, x = 0.6) (pink line). It can be observed that the peaks at 2θ = 25.8°, 38.5°, 48.4°, 55.0°, and 636.6° can be assigned to the anatase TiO_2 (101), (004), (200), (211), and (204) lattice planes, respectively. It is notable that because of the relatively small amount of Ag-Au nanoparticles added and their pattern peak overlap with the TiO_2 (004) peak, the Ag-Au nanoparticles (111) peak is difficult to be observed. Also, because of the similar lattice structures of Au (a = 0.408 nm) and Ag (a = 0.409 nm), it hard to determine the lattice difference between Ag and Au with the XRD technique. Thus, the composition of the composites requires further characterization.

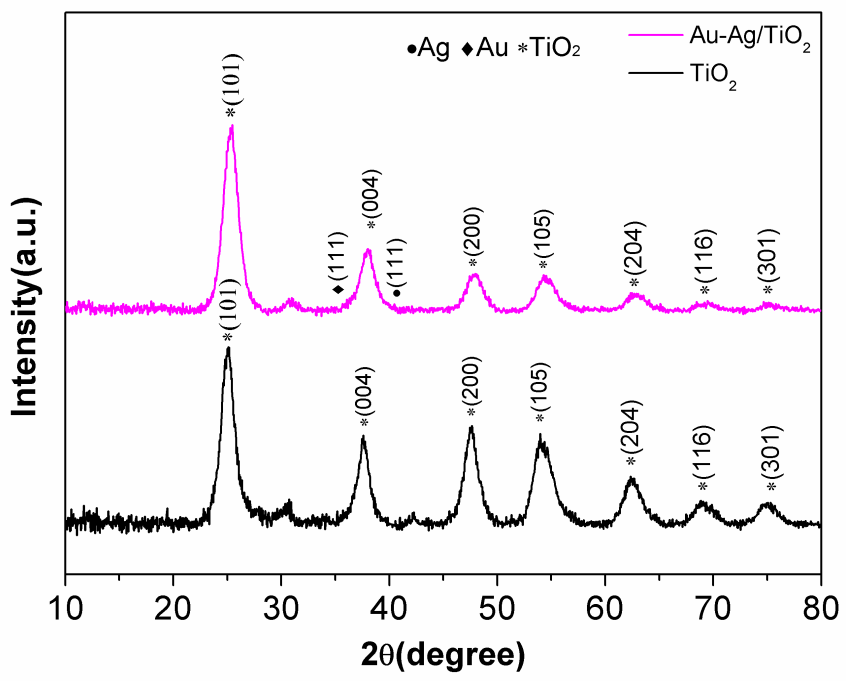

Figure 1. XRD pattern of pure TiO_2 and 1.18 wt% Au-1.07 wt% Ag decorated TiO_2 particles.

2.2. Morphology Study

Figure 2A displays the TEM image of individual Ag-Au co-decorated TiO_2 spheres obtained by loading 1.18 wt% Au and 1.07 wt% Ag. It was determined that the TiO_2 spheres were ~200 nm in diameter, and Au-Ag nanoparticles were uniformly loaded to the surface of TiO_2 spheres. High-resolution TEM images were used to observe more details of the composites. The Ag-Au binary nanoparticles had diameters of 5 to 20 nm as shown in Figure 2B. With further magnification, the lattice fringes of both particles were clearly seen (Figure 2C). The interplanar space of 2.30 Å and 2.36 Å was observed to be indexed to a (111) plane of Au or Ag and a (004) plane of TiO_2, respectively [34,35]. TiO_2 particles were further characterized by backscattered electron SEM imaging, as shown in Figure 3A. The TiO_2 particles were observed as uniform spheres with diameters of 200 nm, which is in agreement with TEM images. The bright little dots (marked by the red arrows in the image) correspond to Au-Ag nanoparticles. Figure 4B shows the EDS spectrum of Au-Ag nanostructure decorated TiO_2 spheres with 0.5% Au and 1.75% Ag. The XRD technique cannot distinguish Ag from Au elements. Therefore, EDS element mapping was used to confirm the composition of the particles. Four elements (Ti, Ag, Au, and O) were scanned and the independent element mappings are displayed in Figure 3C–F, respectively. It was found that Ti and O elements shared and constituted the TiO_2 particles, but the intensity of O element looks stronger than that of Ti element, since their number is double that of the Ti atoms. While Ag and Au elements had a similar distribution, their detection

location was different, indicating metallic Ag-Au binary particles were formed. This suggests that the small 5 to 20 nm particles were Ag-Au.

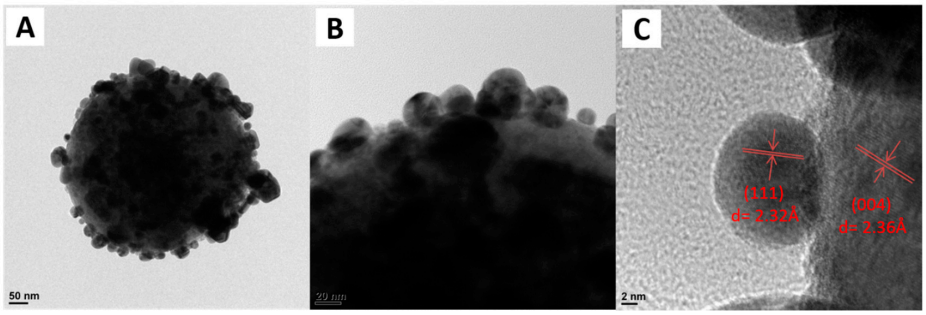

Figure 2. TEM image (**A**) and high resolution TEM image (**B**) and (**C**) of 1.18 wt% Au-1.07 wt% Ag-decorated TiO_2 composites.

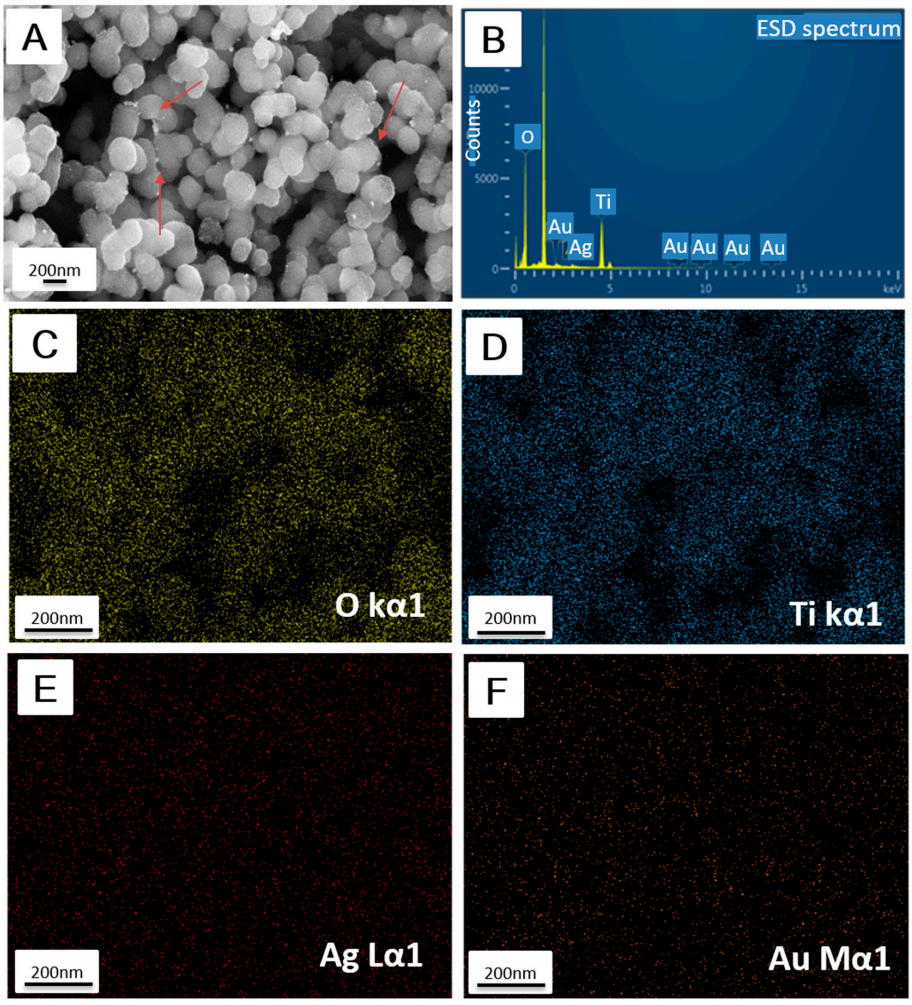

Figure 3. (**A**) SEM image and (**B**) EDS spectra of 1.18 wt% Au-1.07 wt% Ag-decorated TiO_2 composites; (**C**–**F**) EDS mapping analysis of component elements from a SEM image (**A**) of Au-Ag decorated on TiO_2 composites showing the distribution of Ti, O, Ag, and Au.

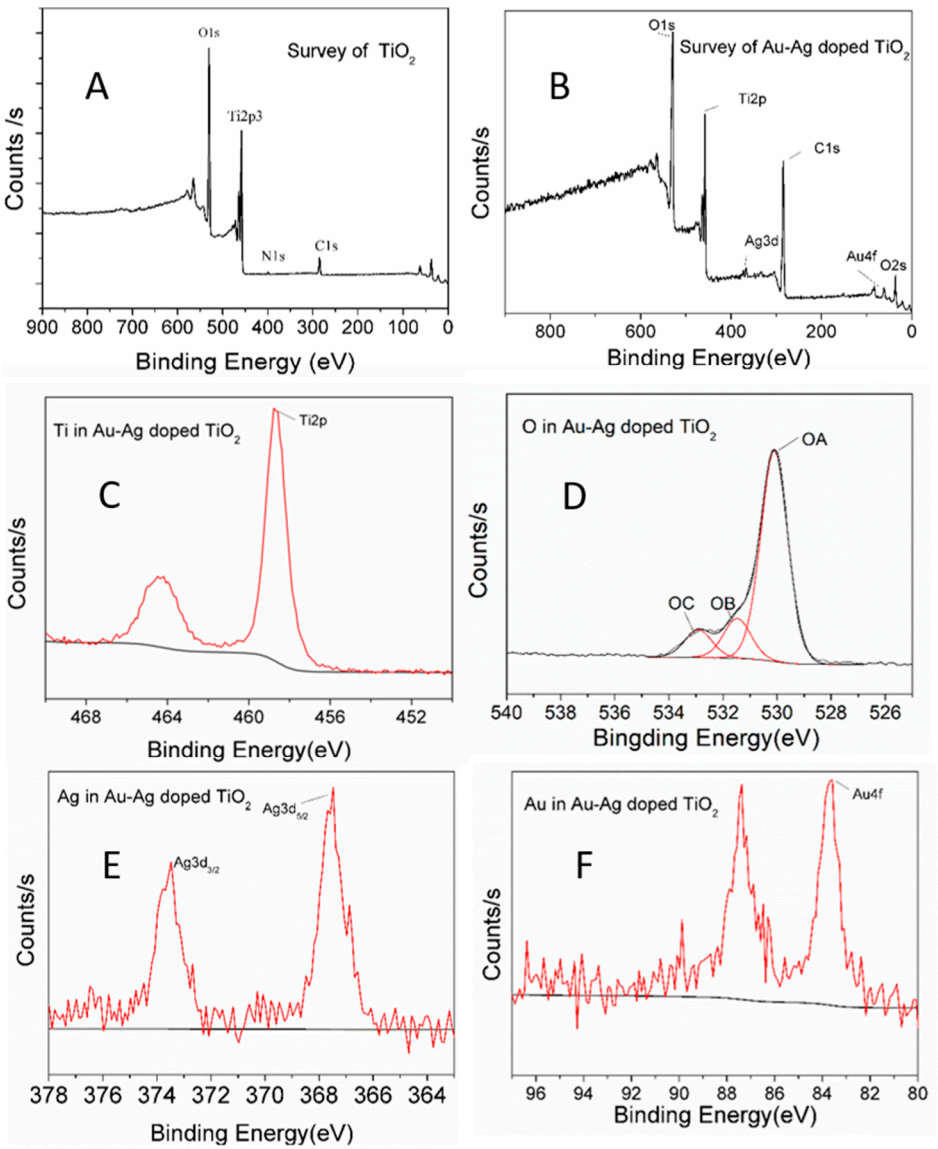

Figure 4. (**A**) XPS spectra of the as-prepared pure TiO_2 particles, and (**B**) Au-Ag-decorated TiO_2 particles ($Au_xAg_{(1-x)}/TiO_2$, x = 0.6); (**C**–**F**) XPS elemental spectra for Ti2p3, O 1s, Ag3d and Au4f in Au-Ag decorated TiO_2 particles.

XPS was introduced to analyze the surface composition of the particles. Being different from EDS characterization. XPS spectra not only shows the elements present but also their valance states. The composition of a particle can then be characterized more accurately. As a control, pure TiO_2 was characterized using XPS. Its survey spectrum is presented in Figure 4A. The binding energies were modified for specimen charging in accordance with the C 1s to 284.8 eV. Both titanium (459.1 eV) and oxygen (530.6 eV) were detected in samples. Figure 4B shows the XPS survey spectrum of Ag-Au co-decorated TiO_2 composites. Extra peaks indexed to Ag 3d and Au 4f were seen that were not seen in pure TiO_2. The Ti 2p core-level spectra displayed two representative peaks at 464.5 and 458.9 eV (Figure 4C) (464.7 and 459.1 eV for pure TiO_2), which can be attributed to the spin-orbital splitting photoelectrons of Ti $2p_{1/2}$ and Ti $2p_{3/2}$ in the Ti^{4+} state. Reports elsewhere had similar findings [36]. The O1s shown in Figure 4D is asymmetric, indicating several oxygen species. The deconvolution peaks of oxygen species at high binding energy (O_C, 532.8 eV) can be assigned to the chemisorbed oxygen species in the surface hydroxyl groups (O–H bond). The other two peaks located at 530.2 and 531.9 eV represent O_A and O_B, respectively. These come from the O^{2-} ions in the TiO_2 and O^- and O^{2-}

ions in the oxygen vacancies-induced defect regions, which mainly contributes to the photocatalytic reaction [37]. The high-resolution XPS signals of Ag and Au in the composite are summarized in Figure 4E,F, respectively. The binding energy of Au $4f_{7/2}$ is 83.7 eV, there is a negative shift of −0.3eV when compared with bulk metallic gold (84.0 eV). Similar results were reported in other studies [38,39]. The shift can be explained by the effect of TiO_2 support. Arrii et al. reported the role of different support materials on the binding energy shifts of Au $4f_{7/2}$. They reported up to −1.1 eV negative shift occurs in the TiO_2 host particles [40]. The similar intensity between Au $4f_{7/2}$ and Au $4f_{5/2}$ suggests an interaction and coexistence between Ag and Au [41]. The Au-Ag bi-metal increases the possibility of Au or Ag losing electrons. Ag $3d_{3/2}$ and Ag $3d_{5/2}$ also shifted to lower values (373.4 eV and 367.5 eV) compared to monometallic Ag (374.2eV and 368.3eV). There was no sign of ionic species and this suggests Ag and Au were attached to the TiO_2 surface.

2.3. Optical Properties

The UV-vis spectra of various samples related to Ag-Au co-decorated TiO_2 particles were measured. Figure 5 presents the UV-vis spectra of the $Au_xAg_{(1-x)}/TiO_2$ (x is the amount of Au in the Ag-Au binary nanoparticles, where x = 0, 0.2, 0.4, 0.6, 0.8 and 1) and the pure TiO_2. The adsorption peak of TiO_2 is located at ~310 nm, which is consistent with our previous study [42]. The absorption peak moves to a longer wavelength by ~80 to 390 nm after decorating Ag nanoparticles (x = 0), and where the amount of Ag loaded is ~2.25 wt. % of TiO_2. As a control test, only loading Au nanoparticles (($Au_xAg_{(1-x)}/TiO_2$), x = 1) leads to a significant red-shift to ~460 nm. This band change indicates that decorating Ag or Au nanoparticles can result in an increase in its adsorption at longer wavelengths such as the visible light region.

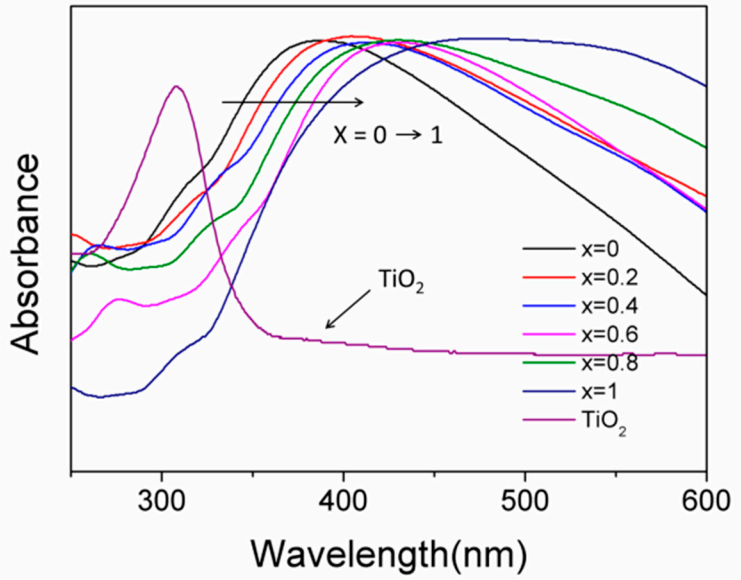

Figure 5. UV–vis spectra of $Au_xAg_{(1-x)}/TiO_2$ composites (x = 0, 0.2, 0.4, 0.6, 0.8, and 1) and the pure TiO_2 spheres.

To obtain tunable absorbance of the photocatalysts, Ag-Au co-decorated TiO_2 spheres with various ratios of Ag to Au (marked as $Au_xAg_{(1-x)}/TiO_2$) were prepared. The optical properties of the different composites were measured, and the results are shown in Figure 5. It is notable that the positions of the maximum absorbance peaks shift to long-wavelength with x. Specifically, when x equals to 0.2, 0.4, 0.6, and 0.8, the positions of the SPR wavelength shifts to 390, 405, 415, 425, and 440 nm, respectively. Thus the surface plasmon resonance absorption can be tuned by controlling the ratios of Ag to Au, as well as the size of Ag or Au nanoparticles [24]. The degree of overlap between the emission of the light source and a particle's UV-vis absorption is indicative of its sunlight photocatalytic activity.

2.4. Specific Surface Area Test

The specific surface area of a composite is another determinant for the functional activities in photocatalysis and those related to the contact surface area. In this study, the specific surface area was estimated for the 1.18 wt% Au 1.07 wt% Ag co-decorated TiO_2 samples. The N_2 adsorption-desorption isotherms and the pore size distribution of the calculations are shown in Figure 6A,B, respectively. The isotherms display a type IV curve, indicating a mesoporous structure. According to the Brumauer-Emmett-Teller formula, the specific surface area of the composite was calculated as ~156.6 m^2/g. This value is about double that measured when the pure TiO_2 spheres were tested (81.8 m^2/g) [42]. This is probably due to a spillover effect [43,44]. The characterized pore size distribution method is based on an adsorption and desorption branch of the isotherm (using the Barrett-Joyner-Halenda) method). The average pore size was calculated as ~3.5 nm (Figure 6B). Therefore, decorating with Au-Ag nanoparticles greatly increases the specific surface area of the composite. This is desirable for the proposed photocatalytic applications.

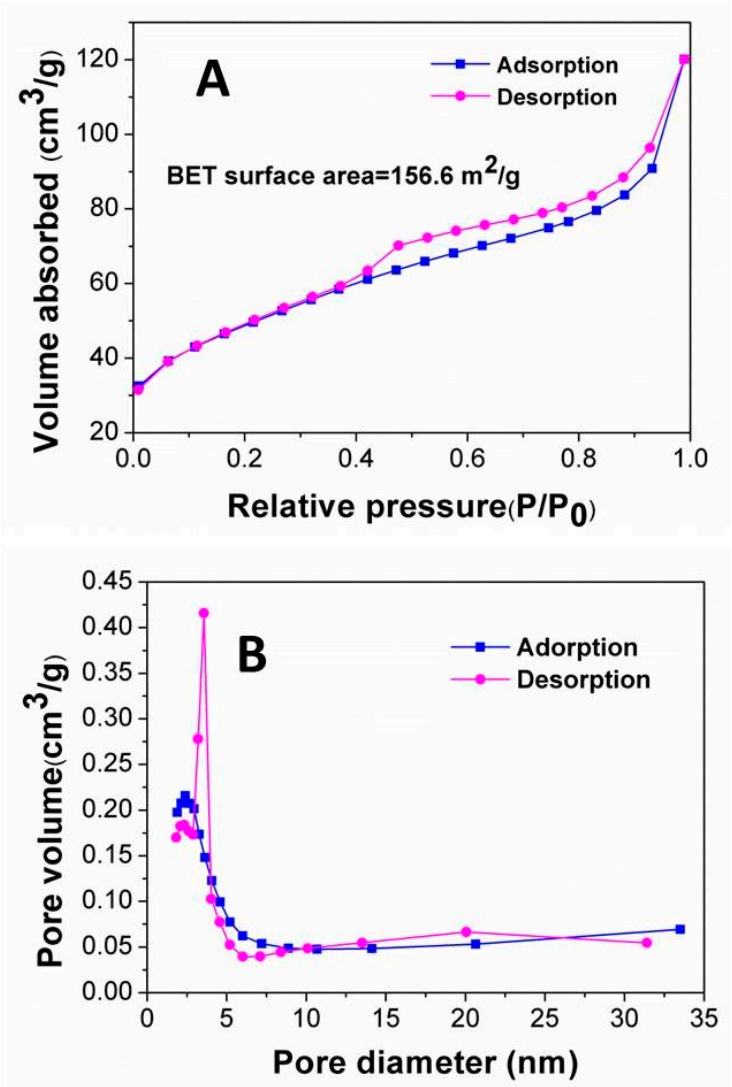

Figure 6. The nitrogen (N_2) adsorption-desorption isotherms (**A**) and pore size distribution (**B**) of 0.5% Au-1.75% Ag decorated TiO_2 composites.

2.5. Photocatalytic Assessment

The photocatalytic performance of the Ag-Au co-decorated TiO_2 particles with various Ag/Au ratios was assessed by testing the degradation of a methylene blue (MB) solution under visible light irradiation. Figure 7A shows the photocatalytic degradation rate of MB with $Au_xAg_{(1-x)}/TiO_2$ (x = 0, 0.2, 0.4, 0.6, 0.8, and 1) and pure TiO_2 particles as a control. The pure TiO_2 particles had a better photo degradation efficiency than commercially available TiO_2 [42]. Before this irradiation test, the MB suspension and photocatalyst mix were left in the dark for 30 min to attain an absorption-desorption equilibrium of MB on the surface of the particles. The commercial TiO_2 spheres had a ~20% degradation rate after 2 h. In contrast, the Ag-decorated TiO_2 spheres (x = 1) had a ~75% degradation rate after 2 h. The Au decorated TiO_2 spheres (x = 0) had a 82% degradation rate after 2 h. The highest degradation rate (~99%) was observed when the composite had an x of 0.6. The reaction rate of the pure TiO_2 particles and the Ag-Au co-decorated TiO_2 spheres with different Ag/Au molar ratios (x) are shown in Figure 7B. $Ag_{0.6}Au_{0.4}/TiO_2$ composite has a superior photocatalytic activity (0.0317 min^{-1}) compared to other $Ag_xAu_{(1-x)}/TiO_2$ composites (from 0.0156 to 0.0252 min^{-1}) and pure TiO_2 nanospheres (0.0023 min^{-1}).

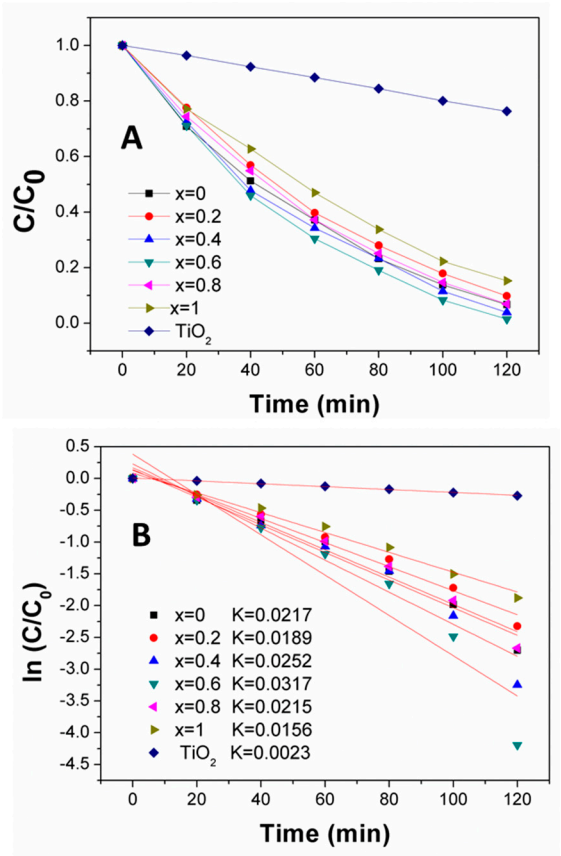

Figure 7. (**A**) Concentration change of methylene blue (MB) in the presence of pure TiO_2 particles, and $Au_xAg_{(1-x)}/TiO_2$ composites with x = 0.2, 0.4, 0.6, 0.8 and 1 under sunlight irradiation. (**B**) Photodegradation rates of the pure TiO_2 particles, and $Au_xAg_{(1-x)}/TiO_2$ composites with x = 0, 0.2, 0.4, 0.6, 0.8 and 1. Reaction rates (k) in the inset are calculated from the linear relationship between ln (C_0/C) and time.

The superior photocatalytic activity would benefit from the suitable ratio of Au and Ag, which could help to reduce the photogenerated electron-hole recombination via modifying the bandgap and trapping the charge carrier [45]. Similarly, Mohsen et al. synthesized the Ag-Au-modified TiO_2 nanotube and investigated the photocatalytic degradation performance toward the MB under visible light, the results reveal that Au-Ag/TiO_2 nanotubes show remarkable enhancement of photocatalytic

activity because of more visible light absorption [46]. Jaspal explored the photocatalytic performance of Ag-doped TiO_2 nanoparticle fabricated by the CTAB-assisted facile wet chemical method and concluded that 100 mL 8 μM aqueous solution of MB can be fully degraded under artificial sunlight within 60 min by using 5 mg Ag-TiO_2 nanoparticles, while 40% degradation was achieved by using the same amount of pure TiO_2 nanoparticles [47]. Reinis et al. also reported a microwave-assisted strategy to prepare Au, Pt, Pd, and Ag-doped TiO_2 nanofibers, the high intensity LED lamp was applied to photodegrade the MB, and the noble metal-doped TiO_2 showed double photocatalytic efficiency in comparison with pure TiO_2 nanofibers. All the above works are in agreement with the trend of our results [48].

Loading noble metal nanoparticles on TiO_2 increases the absorption of visible light through surface plasmon resonance (SPR) and this boosts the photocatalytic activity [6,49,50]. Surface plasmon resonance is a collective oscillation among the conduction band electrons in a metal particle after it is excited by light [51]. When a metal nanoparticle is irradiated with a wavelength of light larger than the particle, redistribution occurs within the particle of the charge density. This modification of a metal particle on a TiO_2 particle by light establishes a coulombic restoring force and prompts a charge density. Au and Ag particles are frequently used in plasmonic composites. Their resonance frequency depends on the shape and size of the host particle, the interactions between the metal and the host material, as well as the local dielectric environment [52].

The recognized mechanism corresponding to SPR and associated photoreactivity is not strictly established. In the present study, the proposed photocatalysis mechanism of Au-Ag/TiO_2 composites is summarized, as shown in Figure 8, the Au/Ag NPs and TiO_2 particles absorb the incident photons, and the electrons in the valence band in TiO_2 are excited afterwards. The excited electrons move to the conductive band, at the same time, the same amount of holes are generated in the valence band. Because of the higher work functions of Ag (4.3 eV) and Au (5.1 eV) compared with that of anatase TiO_2 (3.2 eV), partial excited electrons would transfer from TiO_2 conductive band to the surface-loaded Au or Ag NPs, since the Fermi energy level of noble metal is lower than that of TiO_2. By this way, the electron-hole recombination is restrained. Since the Au-Ag/TiO_2 composites are able to absorb the near-ultraviolet to visible light, this helps to absorb more photons, further excite more electrons within TiO_2, resulting in accumulating more holes. The electrons come up against an oxygen molecule to form superoxide anions ($\cdot O_2$). At the same time, the photo-induced holes were trapped by OH^- to become hydroxyl radicals. Both hydroxyl radicals and superoxide anions would oxidize MB to CO_2 and H_2O. Besides, the photocatalytic reaction rates are strongly dependent on the wavelength of the incident light, for the highest reaction rate, the wavelength of light should cover the range where the intensity of the SPR is the highest [53].

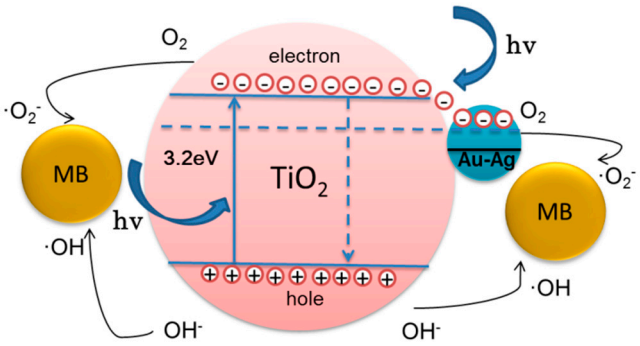

Figure 8. Mechanism of MB photodegradation by Au-Ag decorated TiO_2 composites.

3. Experimental

3.1. Chemicals

Gold (III) chloride trihydrate ($HAuCl_4 \cdot 3H_2O$, 99%), silver nitrate ($AgNO_3$, 97%), sodium borohydride ($NaBH_4$, 99hexylamine ($C_6H_{15}N$ 99%), titanium (IV) butoxide (TBOT 99%), methylene blue ($C_{16}H_{24}ClN_3O_3S$, 97%) and commercial titanium dioxide (TiO_2, P25) were purchased from Sigma Aldrich (Shanghai, China). Silver nitrate ($AgNO_3$, 97%), acetone (C_3H_6O, 99.9%), ethylene glycol (EG, $(CH_2OH)_2$ 97%), ethanol (C_2H_6O, 99.9%) and methylene blue ($C_{16}H_{24}ClN_3O_3S$, 97%) were purchased from Sinopharm chemical reagent Co., Ltd. (Shenyang, China), all reagents were supplied analytical grade and used as received. Ultra-pure water was used whenever water was used.

3.2. Synthesis of TiO_2 Nanoparticles

To prepare TiO_2 nanoparticles, 0.05 mL titanium (IV) butoxide (TBT) was mixed with 10 mL ethylene glycol, followed by vigorous stirring for 8 h at room temperature. Afterwards, 0.05 mL of this mixture (TBT-EG) was added to 10 mL acetone followed by 5 min of gentle rocking. The mix was then held for 1 h to "age." The precipitate formed (a titanium precursor) was collected using a centrifuge (Eppendorf, Beijing, China) set at 3000 rpm for 10 min. The collected particles were dispersed in boiling water and held for 2 h. The as-prepared colloids were collected by centrifuge, then rinsed with alcohol, and dried in an oven set at 60 °C overnight.

3.3. Synthesis of Au-Ag/TiO_2 Composites

To synthesize colloidal Au-Ag/TiO_2, in a typical procedure, 0.01 mM of TiO_2 colloid was added to 15 mL ethylene glycol and stirred until dispersed. Total of 0.01 to 0.06 mL of 0.01 M $AgNO_3$ and 60 µL hexylamine was added to 15 mL TiO_2 that contained an EG suspension. The mixture was magnetically stirred. Then 0.01 to 0.06 mL 0.01 M $HAuCl_4 \cdot 3H_2O$ and 0.05 M $NaBH_4$ was poured into the mixture and held at room temperature for 2 h. The as-prepared colloids were collected by centrifuge, washed with alcohol, and dried for a few hours in vacuum at 60 °C.

3.4. Characterizations

The as-synthesized samples were identified by Phillips X'pert Multipurpose X-ray Diffractometer (MPD 6100, Shimadzu, Shenyang, China) using Cu Kα radiation and a scanning step $2\theta = 0.02°/s$. XPS analysis determines the surface composition of the samples on a Physical Electronics PHI 5000 Versa prob (Kratos Analytical, Manchester, UK) using Al Kα_X-ray source set at 1486 eV. The data were analyzed with XPSPEAK software (version 4.1 Kratos Analytical, Manchester, UK). The morphologies of the as-prepared samples were investigated by TEM (JEOL 1400, Peabody, MA, USA) with an accelerated voltage set at 100 kV. To observe the surface, SEM images were obtained by emission scanning electron microscope (ZEISS, Shanghai, China). High-resolution TEM microscope (HRTEM, FEI Tecnai G20, FEI, Shanghai, China) with an accelerating voltage set at 200 kV was used to study the crystalline structure and its interface. A UV-2600 UV-Vis spectrophotometer (Shimadzu, Shenyang, China) was used to obtain the UV-visible absorption spectrum of samples. The specific surface area and pore size distribution of the samples were measured with a nitrogen physisorption isotherms via a BET process (TriStar 3000, micromeritics Instrument Corporation, Shanghai, China).

3.5. Photocatalytic Test

The photocatalytic performance of Au-Ag/TiO_2 related samples was evaluated through the degradation of MB solution (30 mg/L) with simulated sunlight irradiation via a 300W Xenon lamp (PLS-SXE300C) equipped with an AM 1.5 G total reflection filter (Perfect light, Beijing, China). The intensity of the light was 0.7 W/cm^2. Total of 20 mg of the photocatalyst was added to 100 mL of MB solution to form a concentration of 30 mg/L. Before irradiation, to form an adsorption-desorption

equilibrium, the mix was stirred in the dark for 30 min. During the reaction, the reactor was equipped with a reflux condensation to remove heat. Total of 3 mL of solution was sampled at set time intervals and centrifuged to remove the catalyst particles. The intensity of the absorption peaks of MB was measured with a Shimadzu UV-2600 UV-Vis spectrophotometer (Shimadzu, Shenyang, China) and used to track its concentration.

4. Conclusions

The photocatalytic performance of TiO_2 under visible light was tested by modifying the SPR of Au-Ag nanoparticles that co-decorated its surface. The composites were found to have excellent stability and a large specific surface area. Specifically, colloidal suspensions of Au-Ag co-decorated TiO_2 ($Au_xAg_{(1-x)}/TiO_2$) composites with x in the range of 0 to1 showed an intensive SPR band in the range of 390 to 520 nm visible light. Based on the photocatalytic assessment, the $Au_{0.4}Ag_{0.6}$ co-decorated TiO_2 could generate SPR at 460 nm. This was the best result for the degradation of methylene blue under solar light irradiation. It was better than pure TiO_2 or TiO_2 with other Au/Ag ratios. The SPR induced by Ag-Au co-decoration helped the TiO_2 particles absorb light from the near-ultraviolet to the visible light range. The photoelectrons excited on the conduction band of TiO_2 tend to transfer to the Au-Ag nanoparticles because of the lower fermi level of noble metal. This leads to the efficient separation of photogenerated electron-hole pairs. The method used to make these particles enabled their practical photocatalytic tuning. This work provides a simple way to make efficient solar light-responsive photocatalytic material that could be used for environmental remediation and for energy saving applications.

Author Contributions: X.Y., Y.W., L.Z., and H.F. designed the study. X.Y. and H.F. wrote the paper. Y.W., L.Z., and P.H. carried out experiments and analyzed the data. D.H. carried out XPS experiments and analyzed the data. T.L. revised the English writing. X.A. supervised the whole project and provided the financial support. All authors have read and agreed to the published version of the manuscript.

Funding: This research was funded by National Natural Science Foundation of China (No. 51704070 and No. 51974086). Dezhi Han received the Start-up Foundation for Advanced Talents of Qingdao University of Science and Technology (010022919).

Acknowledgments: We acknowledge the help of the School of Metallurgy (Northeastern University) with the BET surface area measurement and the NEU Microscopy facility for electron microscopy and elemental analysis.

Conflicts of Interest: The authors declare no conflict of interest.

References

1. Fujishima, A.; Zhang, X.; Tryk, D. TiO_2 photocatalysis and related surface phenomena. *Surf. Sci. Rep.* **2008**, *63*, 515–582. [CrossRef]
2. Yao, W.F.; Zhang, B.; Huang, C.P.; Ma, C.; Song, X.L.; Xu, Q.J. Synthesis and characterization of high efficiency and stable Ag_3PO_4/TiO_2 visible light photocatalyst for the degradation of methylene blue and rhodamine B solutions. *J. Mater. Chem.* **2012**, *22*, 4050–4055. [CrossRef]
3. Babu, S.G.; Vinoth, R.; Kumar, D.P.; Shankar, M.V.; Chou, H.L.; Vinodgopal, K.; Neppolian, B. Influence of electron storing, transferring and shuttling assets of reduced graphene oxide at the interfacial copper doped TiO_2 p–n heterojunction for increased hydrogen production. *Nanoscale* **2015**, *7*, 7849–7857. [CrossRef] [PubMed]
4. Yi, J.H.; Huang, L.L.; Wang, H.J.; Yu, H.; Peng, F. AgI/TiO_2 nanobelts monolithic catalyst with enhanced visible light photocatalytic activity. *J. Hazard. Mater.* **2015**, *284*, 207–214. [CrossRef] [PubMed]
5. Pinho, L.; Mosquera, M.J. Photocatalytic activity of TiO_2–SiO_2 nanocomposites applied to buildings: Influence of particle size and loading. *Appl. Catal. B Environ.* **2013**, *134*, 205–221. [CrossRef]
6. Primo, A.; Corma, A.; Garcia, H. Titania supported gold nanoparticles as photocatalyst. *Phys. Chem. Chem. Phys.* **2011**, *13*, 886–910. [CrossRef]
7. Dong, F.; Guo, S.; Wang, H.Q.; Li, X.F.; Wu, Z.B. Enhancement of the Visible Light Photocatalytic Activity of C-Doped TiO2Nanomaterials Prepared by a Green Synthetic Approach. *J. Phys. Chem. C* **2011**, *115*, 13285–13292. [CrossRef]

8. Asahi, R.; Morikawa, T.; Irie, H.; Ohwaki, T. Nitrogen-Doped Titanium Dioxide as Visible-Light-Sensitive Photocatalyst: Designs, Developments, and Prospects. *Chem. Rev.* **2014**, *114*, 9824–9852. [CrossRef]
9. Zimbone, M.; Cacciato, G.; Spitaleri, L.; Egdell, R.G.; Grimaldi, M.G.; Gulino, A. Sb-Doped Titanium Oxide: A Rationale for Its Photocatalytic Activity for Environmental Remediation. *ACS Omega* **2018**, *3*, 11270–11277. [CrossRef]
10. Wang, T.; Shen, D.Y.; Xu, T.; Jiang, R.L. Photocatalytic degradation properties of V-doped TiO2 to automobile exhaust. *Sci. Total Environ.* **2017**, *586*, 347–354. [CrossRef]
11. Banisharif, A.; Khodadadi, A.A.; Mortazavi, Y.; Firooz, A.A.; Beheshtian, J.; Agah, S.; Menbari, S. Highly active Fe_2O_3-doped TiO_2 photocatalyst for degradation of trichloroethylene in air under UV and visible light irradiation: Experimental and computational studies. *Appl. Catal. B Environ.* **2015**, *165*, 209–221. [CrossRef]
12. Cheng, C.; Amini, A.; Zhu, C.; Xu, Z.L.; Song, H.S.; Wang, N. Enhanced photocatalytic performance of TiO_2-ZnO hybrid nanostructures. *Sci. Rep.* **2014**, *4*, 4181. [CrossRef] [PubMed]
13. Zimbone, M.; Cacciato, G.; Boutinguiza, M.; Gulino, A.; Cantarella, M.; Privitera, V.; Grimaldi, M. Hydrogenated black-TiO_x: A facile and scalable synthesis for environmental water purification. *Catal. Today* **2019**, 146–157. [CrossRef]
14. Zhou, X.M.; Liu, G.; Yu, J.G.; Fan, W.H. Surface plasmon resonance-mediated photocatalysis by noble metal-based composites under visible light. *J. Mater. Chem.* **2012**, *22*, 21337–21354. [CrossRef]
15. Linic, S.; Christopher, P.; Ingram, D.B. Plasmonic-metal nanostructures for efficient conversion of solar to chemical energy. *Nat. Mater.* **2011**, *10*, 911–921. [CrossRef]
16. Zhu, Z.N.; Meng, H.F.; Liu, W.J.; Liu, X.F.; Gong, J.X.; Qiu, X.H.; Jiang, L.; Wang, D.; Tang, Z.Y. Superstructures and SERS Properties of Gold Nanocrystals with Different Shapes. *Angew. Chem.* **2011**, *123*, 1593–1596. [CrossRef]
17. Khlebtsov, B.N.; Khlebtsov, N.G. Multipole Plasmons in Metal Nanorods: Scaling Properties and Dependence on Particle Size, Shape, Orientation, and Dielectric Environment. *J. Phys. Chem. C* **2007**, *111*, 11516–11527. [CrossRef]
18. Rycenga, M.; Cobley, C.M.; Zeng, J.; Li, W.Y.; Moran, C.H.; Zhang, Q.; Qin, N.; Xia, Y.N. Controlling the Synthesis and Assembly of Silver Nanostructures for Plasmonic Applications. *Chem. Rev.* **2011**, *111*, 3669–3712. [CrossRef]
19. Xia, Y.N.; Xiong, Y.J.; Lim, B.; Skrabalak, S.E. Shape-controlled synthesis of metal nanocrystals: Simple chemistry meets complex physics? *Angew. Chem. Int. Ed.* **2009**, *48*, 60–103. [CrossRef]
20. Grzelczak, M.; Pérez-Juste, J.; Mulvaney, P.; Liz-Marzán, L.M. Shape control in gold nanoparticle synthesis. *Chem. Soc. Rev.* **2008**, *37*, 1783–1791. [CrossRef]
21. Kimling, J.; Maier, M.; Okenve, B.; Kotaidis, V.; Ballot, H.; Plech, A. Turkevich Method for Gold Nanoparticle Synthesis Revisited. *J. Phys. Chem. B* **2006**, *110*, 15700–15707. [CrossRef] [PubMed]
22. Sánchez-Iglesias, A.; Grzelczak, M.; Perez-Juste, J.; Liz-Marzán, L.M. Binary Self-Assembly of Gold Nanowires with Nanospheres and Nanorods. *Angew. Chem. Int. Ed.* **2010**, *49*, 9985–9989. [CrossRef] [PubMed]
23. Liz-Marzán, L.M. Tailoring Surface Plasmons through the Morphology and Assembly of Metal Nanoparticles. *Langmuir* **2006**, *22*, 32–41. [CrossRef] [PubMed]
24. Verbruggen, S.W.; Keulemans, M.; Martens, J.A.; Lenaerts, S. Predicting the Surface Plasmon Resonance Wavelength of Gold–Silver Alloy Nanoparticles. *J. Phys. Chem. C* **2013**, *117*, 19142–19145. [CrossRef]
25. Ingram, D.B.; Christopher, P.; Bauer, J.L.; Linic, S. Predictive Model for the Design of Plasmonic Metal/Semiconductor Composite Photocatalysts. *ACS Catal.* **2011**, *1*, 1441–1447. [CrossRef]
26. Sun, Y.G.; Xia, Y.N. Shape-Controlled Synthesis of Gold and Silver Nanoparticles. *Science* **2002**, *298*, 2176–2179. [CrossRef]
27. Kim, F.; Song, J.H.; Yang, P.D. Photochemical Synthesis of Gold Nanorods. *J. Am. Chem. Soc.* **2002**, *124*, 14316–14317. [CrossRef]
28. Wang, X.; Zhuang, J.; Peng, Q.; Li, Y.D. A general strategy for nanocrystal synthesis. *Nature* **2005**, *437*, 121–124. [CrossRef]
29. Huang, J.L.; Li, Q.B.; Sun, D.H.; Lu, Y.H.; Su, Y.B.; Yang, X.; Wang, H.X.; Wang, Y.P.; Shao, W.Y.; He, N.; et al. Biosynthesis of silver and gold nanoparticles by novel sundriedCinnamomum camphoraleaf. *Nanotechnology* **2007**, *18*. [CrossRef]
30. Mallin, M.P.; Murphy, C.J. Solution-Phase Synthesis of Sub-10 nm Au−Ag Alloy Nanoparticles. *Nano Lett.* **2002**, *2*, 1235–1237. [CrossRef]

31. Malathi, S.; Ezhilarasu, T.; Abiraman, T.; Balasubramanian, S. One pot green synthesis of Ag, Au and Au–Ag alloy nanoparticles using isonicotinic acid hydrazide and starch. *Carbohydr. Polym.* **2014**, *111*, 734–743. [CrossRef] [PubMed]
32. Wang, C.; Yin, H.F.; Chan, R.; Peng, S.; Dai, S.; Sun, S.H. One-Pot Synthesis of Oleylamine Coated AuAg Alloy NPs and Their Catalysis for CO Oxidation. *Chem. Mater.* **2009**, *21*, 433–435. [CrossRef]
33. Liu, S.; Chen, G.Y.; Prasad, P.N.; Swihart, M.T. Synthesis of Monodisperse Au, Ag, and Au–Ag Alloy Nanoparticles with Tunable Size and Surface Plasmon Resonance Frequency. *Chem. Mater.* **2011**, *23*, 4098–4101. [CrossRef]
34. Fu, H.T.; Sun, S.Y.; Yang, X.H.; Li, W.F.; An, X.Z.; Zhang, H.; Dong, Y.; Jiang, X.C.; Yu, A.B. A facile coating method to construct uniform porous α-Fe_2O_3@TiO_2 core-shell nanostructures with enhanced solar light photocatalytic activity. *Powder Technol.* **2018**, *328*, 389–396. [CrossRef]
35. Qiu, G.Y.; Ng, S.P.; Wu, C.M.L. Bimetallic Au-Ag alloy nanoislands for highly sensitive localized surface plasmon resonance biosensing. *Sens. Actuators B Chem.* **2018**, *265*, 459–467. [CrossRef]
36. Millesi, S.; Nigro, R.L.; Pedroni, M.; Speghini, A.; Gulino, A. Photoexcited Porphyrins Functionalizing TiO_2 and SnO_2 Nanocrystals. *J. Phys. Chem. C* **2015**, *119*, 23743–23751. [CrossRef]
37. Taverner, A.E.; Gulino, A.; Egdell, R.G.; Tate, T.J. A photoemission study of electron states in Sb-ion implanted TiO_2(110). *Appl. Surf. Sci.* **1995**, *90*, 383–387. [CrossRef]
38. Kaminker, R.; Lahav, M.; Altman, M.; Evmenenko, G.; Dutta, P.; Gulino, A.; Van Der Boom, M.E. Surface-confined core–shell structures based on gold nanoparticles and metal–organic networks. *Chem. Commun.* **2014**, *50*, 4635–4638. [CrossRef]
39. Yuan, C.L.; Wei, W.Y.; Mei, Y.X.; Luo, X.F.; Lei, W. A new approach for fabricating Au-Ag alloy nanoparticles confined in Al_2O_3 matrix. *Mater. Lett.* **2017**, *190*, 248–251. [CrossRef]
40. Arrii, S.; Morfin, F.; Renouprez, A.J.; Rousset, J.L. Oxidation of CO on Gold Supported Catalysts Prepared by Laser Vaporization: Direct Evidence of Support Contribution. *J. Am. Chem. Soc.* **2004**, *126*, 1199–1205. [CrossRef]
41. Wang, A.Q.; Liu, J.H.; Lin, S.D.; Lin, T.S.; Mou, C.Y. A novel efficient Au–Ag alloy catalyst system: Preparation, activity, and characterization. *J. Catal.* **2005**, *233*, 186–197. [CrossRef]
42. Yang, X.H.; Fu, H.T.; Yu, A.B.; Jiang, X.C. Large-surface mesoporous TiO_2 nanoparticles: Synthesis, growth and photocatalytic performance. *J. Colloid Interface Sci.* **2012**, *387*, 74–83. [CrossRef] [PubMed]
43. Xing, R.Q.; Xu, L.; Song, J.; Zhou, C.Y.; Li, Q.L.; Liu, D.L.; Song, H.W. Preparation and Gas Sensing Properties of In_2O_3/Au Nanorods for Detection of Volatile Organic Compounds in Exhaled Breath. *Sci. Rep.* **2015**, *5*, 10717. [CrossRef] [PubMed]
44. Xing, R.Q.; Li, Q.L.; Zhang, J.H.; Xia, L.; Song, J.; Xu, L.; Xie, Y.; Song, H.W. Au-modified three-dimensional In_2O_3 inverse opals: Synthesis and improved performance for acetone sensing toward diagnosis of diabetes. *Nanoscale* **2015**, *7*, 13051–13060. [CrossRef] [PubMed]
45. Li, P.; Wei, Z.; Wu, T.; Peng, Q.; Li, Y.D. Au−ZnO Hybrid Nanopyramids and Their Photocatalytic Properties. *J. Am. Chem. Soc.* **2011**, *133*, 5660–5663. [CrossRef] [PubMed]
46. Afsari, M.; Youzbashi, A.A.; Nuranian, H.; Zahraee, S.M. Remarkable improvement of visible light photocatalytic activity of TiO_2 nanotubes doped sequentially with noble metals for removing of organic and microbial pollutants. *Mater. Res. Bull.* **2017**, *94*, 15–21. [CrossRef]
47. Singh, J.; Tripathi, N.; Mohapatra, S. Synthesis of Ag–TiO_2 hybrid nanoparticles with enhanced photocatalytic activity by a facile wet chemical method. *Nano Struct. Nano Objects* **2019**, *18*, 100266. [CrossRef]
48. Drunka, R.; Grabis, J.; Krumina, A. Preparation of Au, Pt, Pd and Ag Doped TiO_2 Nanofibers and their Photocatalytic Properties under LED Illumination. *Key Eng. Mater.* **2018**, *762*, 283–287. [CrossRef]
49. Lan, J.Y.; Zhou, X.M.; Liu, G.; Yu, J.G.; Zhang, J.C.; Zhi, L.J.; Nie, G.J. Enhancing photocatalytic activity of one-dimensional $KNbO_3$ nanowires by Au nanoparticles under ultraviolet and visible-light. *Nanoscale* **2011**, *3*, 5161–5167. [CrossRef]
50. Naya, S.I.; Teranishi, M.; Isobe, T.; Tada, H. Light wavelength-switchable photocatalytic reaction by gold nanoparticle-loaded titanium(iv) dioxide. *Chem. Commun.* **2010**, *46*, 815–817. [CrossRef]
51. Ghosh, S.K.; Pal, T. Interparticle Coupling Effect on the Surface Plasmon Resonance of Gold Nanoparticles: From Theory to Applications. *Chem. Rev.* **2007**, *107*, 4797–4862. [CrossRef] [PubMed]

52. Palmisano, G.; García-López, E.; Marci, G.; Loddo, V.; Yurdakal, S.; Augugliaro, V.; Palmisano, L. Advances in selective conversions by heterogeneous photocatalysis. *Chem. Commun.* **2010**, *46*, 7074–7089. [CrossRef] [PubMed]
53. Christopher, P.; Xin, H.L.; Linic, S. Visible-light-enhanced catalytic oxidation reactions on plasmonic silver nanostructures. *Nat. Chem.* **2011**, *3*, 467–472. [CrossRef] [PubMed]